JOURNAL OF PROPULSION AND POWER
Vol. 24, No. 1, January–February 2008

Effects of Tip Clearance on Aerodynamic Damping in a Linear Turbine Cascade

Xiuquan Huang* and Li He†
University of Durham, Durham, England DH1 3LE, United Kingdom
and
David L. Bell‡
ALSTOM Power (UK) Ltd, Rugby, England CV21 2NH, United Kingdom

DOI: 10.2514/1.25174

This paper documents an investigation into unsteady flow in a three-dimensional oscillating turbine cascade with emphasis on the influence of tip clearance. Systematic experimental measurements were acquired on a low-speed turbine cascade rig. The cascade consists of seven prismatic turbine blades, with the middle blade being driven to oscillate in a three-dimensional bending/flapping mode. Blades were instrumented with pressure tappings at six spanwise sections to facilitate three-dimensional steady and unsteady pressure measurements on the blade surface. The steady pressure measurements are complemented by computational fluid dynamics simulations. Both are in good agreement and indicate a marked local pressure drop at 70–90%C on the suction surface resulting from the tip-clearance vortex. The measured unsteady pressure shows that at a small tip clearance (1.25–2.5%C), the tip-clearance flow generates a stabilizing contribution around the midchord on the suction surface near the tip. This behavior is in line with a quasi-steady analysis. Whereas at a large tip clearance (5%C), a dominant destabilizing effect is observed around 80%C on the suction surface, which is associated with a well developed tip-clearance vortex.

Nomenclature

A_f	=	amplitude of the unsteady force F
A_x	=	bending amplitude, nondimensionalized with chord
Ap_m	=	amplitude of the mth harmonic pressure
C	=	blade chord length
Cax	=	axial blade chord length
Cp	=	blade surface pressure coefficient, $Cp = (P - P_2)/(P_{01} - P_2)$
$\lvert Cp_m \rvert$	=	amplitude of the mth harmonic pressure coefficient, $\lvert Cp_m \rvert = Ap_m/(P_{01} - P_2)/Ax_{\text{tip}}$
F	=	unsteady force
h	=	blade span, m
k	=	reduced frequency, $k = \omega C/V_{\text{ref}}$
P_{01}	=	inlet stagnation pressure
P_2	=	exit static pressure
Re	=	Reynolds number
S	=	pitch length
V_{ref}	=	reference (isentropic exit) velocity, m/s, $V_{\text{ref}} = \sqrt{2(P_{01} - P_2)/\rho}$
X	=	axial coordinate, m
Y	=	circumferential coordinate, m
Z	=	spanwise coordinate, m
ξ	=	aerodynamic damping coefficient
σ	=	interblade phase angle, deg
ϕ	=	phase angle, deg
ω	=	angular frequency, rad/s

Subscripts

l	=	local
m	=	mth harmonic
tip	=	blade tip
1	=	inlet parameter, first harmonic
2	=	exit parameter, second harmonic

Received 15 May 2006; revision received 9 July 2007; accepted for publication 15 July 2007.

*Ph.D. Candidate, School of Engineering.
†Professor, Thermo-Fluid Dynamics, School of Engineering.
‡Principal Engineer, Aerodynamics Group, Newbold Road.

I. Introduction

THE design of last stage rotor blades in low pressure steam turbines presents a significant challenge in terms of aeromechanical design, due to their high aspect ratio, high operating pressure ratio, and relatively low natural frequencies. This type of rotor blade is often unshrouded, and the flow is characterized by a strong tip-clearance jet. However, very little is known about the influence of the tip-clearance flow on turbine blade flutter.

Bell and He [1] presented three-dimensional test data for a single turbine blade oscillating in a profiled channel. Their results concerning the influence of tip leakage showed a consistent variation in the amplitude of the unsteady pressure response with changes in tip gap. Unfortunately, this study neglects the blade-to-blade interference, which is an important characteristic of turbomachinery blade flutter. Norryd and Bölcs [2] have also reported an experimental investigation concerning the influence of tip clearance on the steady and unsteady blade surface pressure response in a linear turbine cascade. The influence of a change in tip clearance on both the steady and unsteady blade surface pressure distribution is observed at midspan. Unfortunately, the instrumentation was limited to the midspan section in this study.

In a study of fan flutter by Sanders et al. [3], tip-clearance effects were modeled by using a periodic boundary across the nongridded region between the blade tip and the outer casing. Their results revealed that the unsteady aerodynamics in the tip region of the fan was influenced by clearance effects to a much larger extent than the time-average flowfield. Overall, the impact of tip clearance on aeroelastic stability has not been comprehensively researched, resulting in rather limited understanding of the physical flow behavior and its importance. It is conventional practice to employ a "tuned cascade mode" in blade flutter experiments and numerical predictions, that is to say, all blades would oscillate in identical frequency and amplitude but with a constant interblade phase angle. Recently, an "influence coefficient method" has been widely used to obtain unsteady aerodynamic response in oscillating cascades, as explained by Hanamura et al. [4], Crawley [5], Fransson [6], Buffum and Fleeter [7], Körbächer and Bölcs [8], He [9], Nowinski and

Panovsky [10], Yang and He [11] and Vogt [12]. In this method, only the reference blade is oscillating and the influence coefficients (unsteady pressure) measured on the reference blade and its neighbors are linearly superimposed to obtain the tuned cascade data. It has been shown by Crawley [5] that both tuned cascade mode and influence coefficient method give the same aeroelastic formulation. This finding has been experimentally confirmed by Körbächer and Bölcs [8] and Nowinski and Panovsky [10]. The application of the influence coefficient method enables a much simplified experimental setup. Nevertheless, it should be noted that the influence coefficient method and the tuned cascade mode are equivalent only under the assumption of linear superposition.

The purpose of the present investigation is to experimentally examine the influence of tip-clearance flow on turbine blade flutter using the influence coefficient method. The tip clearance considered is up to $5\%C$. Additionally, the test data produced during the course of this study can serve the validation purpose in the further development of computational modelling techniques.

II. Experimental Techniques

A. Low-Speed Test Rig

All the experimental results presented in this paper were obtained from a linear turbine test cascade, which is shown in Fig. 1. Airflow was delivered to this test cascade by a low-speed, open-type wind tunnel [11], which has a rectangular exhaust cross-section of 250×800 mm. In this wind tunnel, the nonuniform discharge from a centrifugal fan is diffused into a large settling chamber, driven through a shaped contraction (contraction ratio of 7.5:1), and delivered to the test turbine cascade. In this setup, uniform flow is developed at the inlet to the working section, through appropriate design of the contraction profile and the deployment of screens and honeycomb before and after the contraction, respectively.

The turbine test cascade consists of seven prismatic turbine blades, Perspex sidewalls, and a wooden frame. Perspex is used at the two sidewalls to provide visual access to the turbine cascade. The blade profile is a bespoke, low-speed design that was developed for the purposes of the present investigation. The cascade data and operational conditions are summarized in Table 1. The top and bottom walls of the cascade were profiled to simulate the two adjacent blades in the cascade; therefore, eight blade passages were formed, with four passages on each side of the middle reference blade. Bleed slots were located at one chord length upstream of blades to break down the boundary layer development on the sidewalls, whereas no such effort was made to remove the boundary layer on the profiled top and bottom walls. Two adjustable tail boards, acting as the extension of the top and bottom walls, were used to help establish blade-to-blade periodicity. To achieve a three-dimensional bending/flapping condition, the reference (central) blade was hinged at the hub end and driven in at the tip end. This allowed a linear variation in bending amplitude along the span. A sinusoidal oscillation rate was enforced by using a single bar crank connection between a dc motor shaft and a rod protruding from the blade tip. Because the hinge at the hub was mounted outside the test section, it should be noted that a small displacement was introduced to the hub of the oscillating blade.

Table 1 Cascade data and operation conditions

Blade chord, C	0.143 m
Blade span, h	0.180 m
Pitch length, S	0.100 m
Stagger angle	40.0 deg
Inlet flow angle	0.0 deg
Deflection angle	70 deg
Vibration mode	First bending, normal to absolute chord
Tip clearances	0.0, 1.25, 2.5, 5.0%C
Bending amplitude	3%C at tip, 0.3%C at hub
Exit isentropic velocity	23.5 m/s
Reynolds number, Re	2.2×10^5
Reduced frequency, k	0.4
Nominal frequency, f	10.3 Hz

For all tip-clearance configurations, the distance between the hub and tip walls was held constant for all blades in the cascade. On the hub (side) wall, profile slots were located to allow the blades to be translated through the end wall, to vary the tip clearance. In this kind of tip-clearance arrangement, it should be observed that the exact blade height is different from one tip clearance to another.

B. Instrumentation, Data Acquisition, and Reduction

The oscillating blade and one nonoscillating blade were instrumented with pressure tappings at six spanwise sections (10, 30, 50, 70, 80, and 95% span). At each spanwise section, 14 pressure tappings were located on the suction surface (SS) and 10 on the pressure surface (PS), as indicated in Fig. 2. In total, there are 144 tappings on each blade surface. These pressure tappings were used for both steady and unsteady pressure measurements. The instrumented nonoscillating blade was interchangeable with all other stationary blades, thereby enabling both steady and unsteady pressure measurements at all blade positions in the cascade.

In this low-speed test facility, realistic reduced frequencies were achieved at low frequencies of blade vibration. For example, a nominal frequency of 10.3 Hz here is equivalent to a reduced frequency of 0.4, which is based on the blade chord and exit isentropic velocity. This made it possible for the unsteady pressure signals to be recorded with off-board pressure transducers. The test rig was equipped with five off-board pressure transducers (Sensym 142C01D, 0–1 psi range with a sensitivity of 5 V/psi), so that a total of 30 sets of measurements were required for each blade in one test. Unsteady signals from the transducers were recorded on a PC through an Amplicon PC30G data-logging card. The unsteady pressure acquisition procedure was synchronized by a signal from an optical Schmitt trigger.

The unsteady pressure signals were ensemble averaged over 150 periods. The ensemble-averaged unsteady pressure signals were reduced into their harmonic components using a Fourier series. To correct the unsteady pressure signal for phase shift and attenuation along the tubing lengths, a tubing transfer function (TTF) scheme,

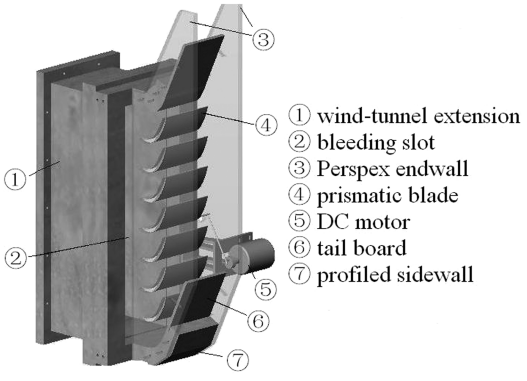

Fig. 1 Turbine test cascade.

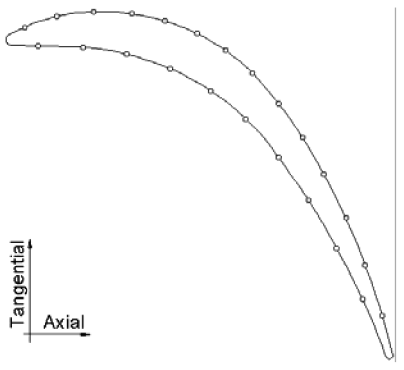

Fig. 2 Pressure tappings.

proposed by Irwin et al. [13], was applied. The present application of the TTF method follows the procedure of Yang and He [11] and Sims-Williams [14].

Once the influence coefficients were obtained on each individual blade, they were superimposed to construct the tuned cascade data by using the influence coefficient method. The validity of the method for this case has been validated by examining the convergence of influence coefficients on those blades away from the central oscillating blade, and the linearity of the unsteady pressures at different oscillation amplitudes. As described earlier, all influence coefficients have been reduced into their harmonic components. Accordingly, the mth harmonic component Cp_m for a tuned cascade can be expressed as a sum of the mth harmonic components $Cp_m(n)$ of influence coefficients from all seven blades:

$$Cp_m = \sum_{n=-3}^{3} Cp_m(n) e^{-in\sigma} \tag{1}$$

where σ is the interblade phase angle and n is the blade index number. The sign convention for the interblade phase angle is such that a negative interblade phase angle corresponds to a backward traveling wave mode.

C. Experimental Errors and Repeatability

The correction of tubing distortion induced by the off-board measuring system has been discussed in Sec. II.B. To justify the neglect of influence away from blade pair ±2 when using the influence coefficient method in a linear cascade experiment, the basic requirement is that the unsteady pressure response is to attenuate quickly away from the oscillating blade in the pitchwise direction. Figure 3 shows the global aerodynamic damping contributions from the central five blades at an interblade phase angle (IBPA) of 0 deg. It is evident that aerodynamic coupling effects are mainly from the immediate neighbors (blades ±1) of the middle reference blade, whereas the contributions from blades ±2 are of negligible magnitude.

Despite the ensemble-averaging process employed, the overall random errors introduced by the complex procedures for unsteady pressure measurements need to be addressed further. To this end, a series of tests were performed to evaluate the experimental errors and repeatability. In these tests, five tappings were chosen from the 70% span of the oscillating blade to provide a representative range of unsteady pressure response. For each tapping, 40 sets of measurements were obtained through the experimental procedure described in Sec. II.B. The measurements showed that the deviation from the mean values fell within a range of ±0.08 for the nondimensional amplitude of the first harmonic pressure and ±5 deg for the phase angle. The corresponding overall standard deviation is below 0.029 in amplitude and 1.95 deg in phase angle, indicating an excellent level of repeatability.

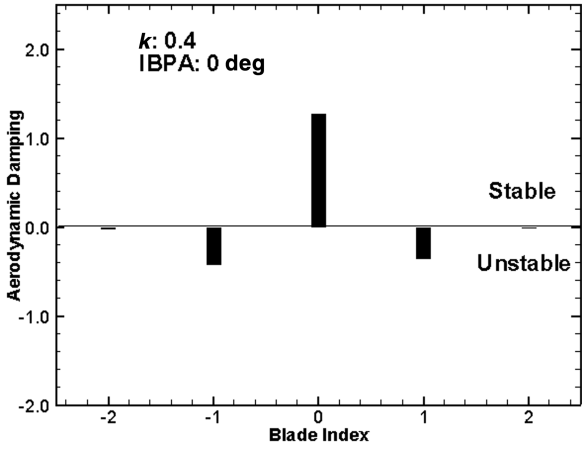

Fig. 3 Experimental test for pitchwise convergence; aerodamping contribution from five central blades (zero tip clearance, K = 0.4, IBPA = 0 deg).

III. Results

A. Steady Flow

Steady flow results are presented in this section. These include steady measurements and a numerical study. The numerical tool is employed here to examine the local tip-clearance flow structure, which is otherwise less accessible, to complement the steady-state surface pressure measurements and help understanding. The computational fluid dynamics (CFD) code used for this purpose, TF3D, solves the three-dimensional, Reynolds averaged, Navier–Stokes equations using a conventional time-marching finite volume scheme. A detailed description of this CFD code and the methods it employs can be found in [15]. Normally, an extra mesh block is required at the blade tip to simulate the tip-clearance flow. To avoid the complexity of employing a multiblock mesh solver, the blade tip is rounded and the gap is filled by a simple H-type mesh, similar to that used in Dawes [16]. It is recognized that detailed resolution of the tip-clearance flow structure may not be possible to obtain when using this grid technique. However, numerous studies [16–19] have shown that the main flow structures and impacts of tip leakage can be adequately captured by this tip treatment. In addition, it should also be recognized that the blade profile used for the purposes of this investigation has a narrow cross section. The mesh used in the calculations is shown in Fig. 4. The overall mesh dimensions were $107 \times 41 \times 51$ nodes, with 3, 6, and 11 cells used in the spanwise direction to resolve the tip clearance for the 1.25, 2.5, and 5.0%C tip clearances, respectively. Although not shown here, a mesh convergence study indicated that the mesh density employed was sufficient to resolve the flow concerned. It is well known that the density based compressible flow solver is unsuitable to calculate the flow of very low Mach number. The flow velocity was therefore elevated to avoid this difficulty. The isentropic exit Mach number prescribed in the calculations was 0.3, at which the flow compressibility effects are considered to be negligible. The calculations were run at the experimental Reynolds number, 2.2×10^5.

Figure 5 shows the steady-state pressure at midspan and 95% span sections of the middle blade, with tip clearances of 0, 1.25, 2.5, and 5%C. Although not shown here, it should be noted that good blade-to-blade periodicity was achieved for the steady flow in the experiment. At zero tip clearance, shown in Fig. 5a, the steady pressure at 95% span exhibits a rather small difference from that at midspan. This indicates that the flow through the linear cascade is largely of a two-dimensional nature if there is no tip clearance. This feature is also predicted by the calculation. When a tip clearance is present, an unloading on the suction surface in the frontal region and a reloading toward the rear are clearly observed at 95% span. On the pressure surface, the unloading manifests itself in a lower Cp and the

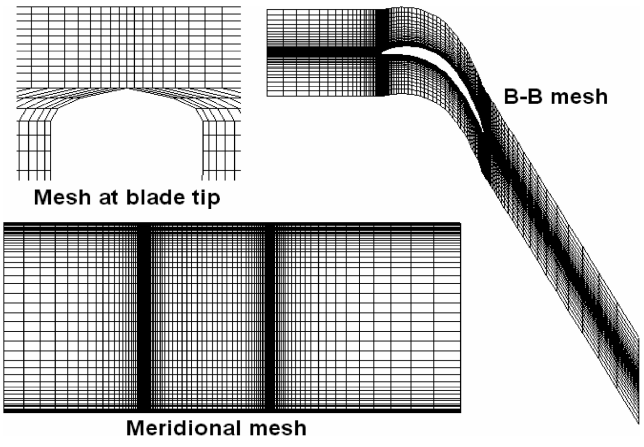

Fig. 4 Computational mesh.

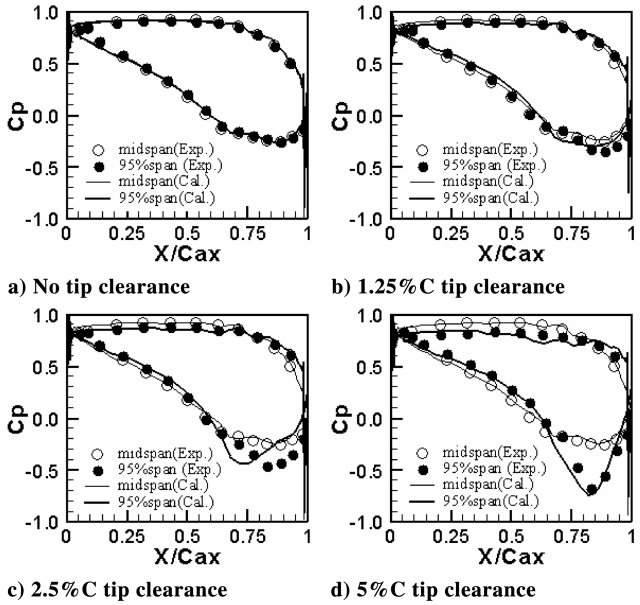

a) No tip clearance b) 1.25%C tip clearance

c) 2.5%C tip clearance d) 5%C tip clearance

Fig. 5 Blade steady pressure distribution.

reloading in a higher Cp, whereas on the suction surface, the trend for change in Cp with unloading and reloading is reversed. When the size of tip clearance is increased, the strengths of unloading and reloading are accordingly increased. Generally, these regions of unloading and reloading are well predicted by the CFD calculations (Figs. 5b–5d), demonstrating that the simple tip-clearance model is able to capture the main features of the steady tip-clearance flow.

The clear low pressure peak around 80%C on the suction surface, shown in Fig. 5, indicates a strong influence of the local tip-clearance flow structure. To help understanding of this flow behavior, CFD results are presented in Fig. 6 in the form of contour plots (entropy and static pressure) and secondary velocity vectors at 80% axial chord. The high loss core [low value of the entropy parameter, $\exp(-\Delta S/R)$] is seen to coincide with the center of the tip-clearance vortex. Notable flow turning over the tip can be observed with associated low static pressures locally. This tip vortex related turning and an associated low pressure region are most evident at the largest clearance gap (Fig. 6c), although interestingly the pitchwise extent of the vortex at this condition is the smallest compared to those at smaller tip gaps. The pressure contours (Fig. 6, right) also illustrate the radial extension of the steady reloading, which is directly associated with the behaviors of tip-clearance vortex. The largest reloading (reduction of pressure on the suction surface) certainly results from the strongest flow rolling up (Fig. 6c), which occurs at the largest tip clearance. As will be seen later, the tip-clearance vortex and its associated local loading redistributions in the steady flow will have a significant bearing on the local unsteady flow and aeroelastic stability.

B. Unsteady Results

The unsteady measurement results for the three tip-clearance settings are presented here and analyzed through comparison with the nominal setting of zero tip clearance. A clear picture of unsteady flow for the nominal case helps discriminate the unsteady response associated with the tip-clearance flow. Therefore, unsteady results

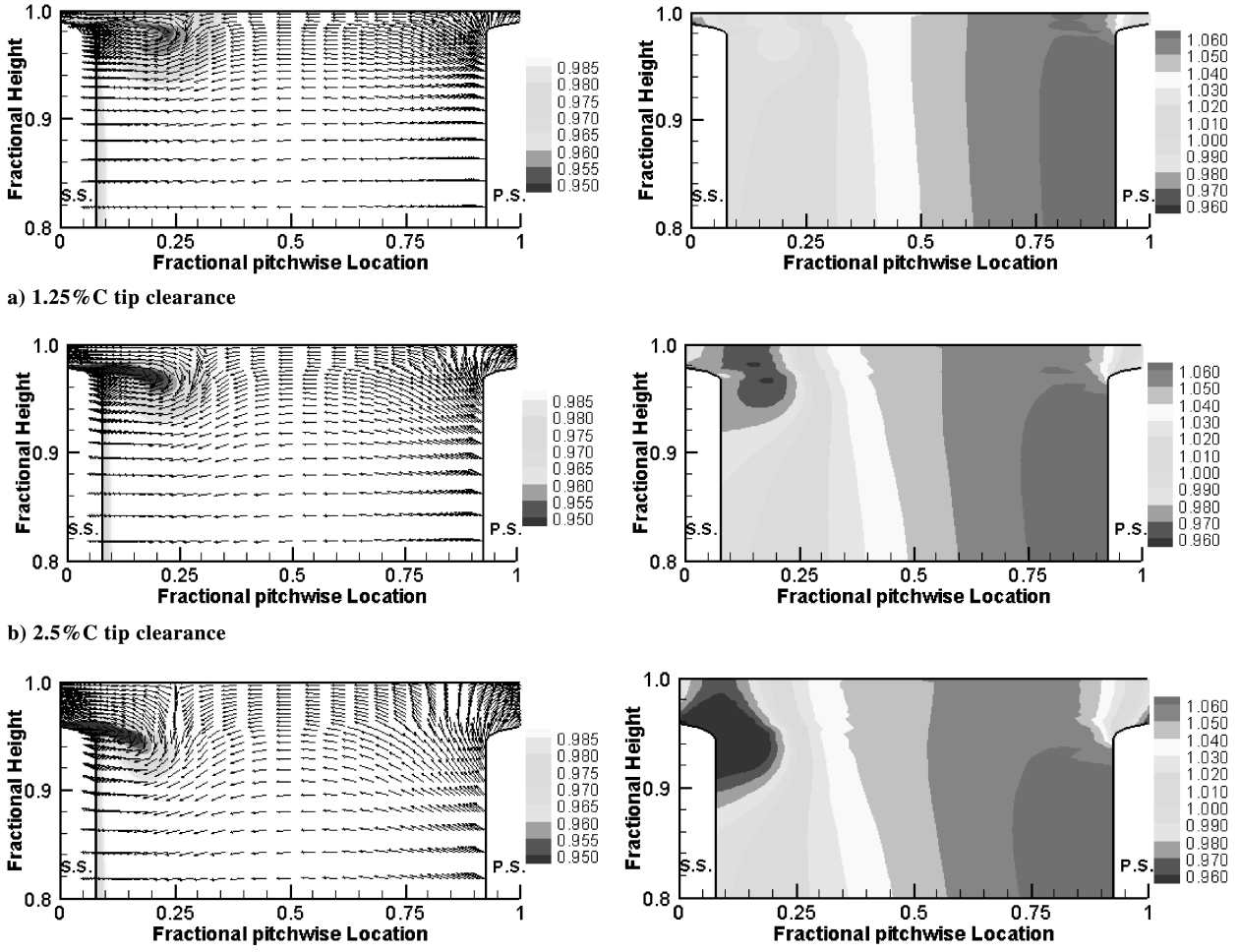

a) 1.25%C tip clearance

b) 2.5%C tip clearance

c) 5%C tip clearance

Fig. 6 Entropy [$\exp(-\Delta S/R)$] contours with velocity vectors (left) and static pressure contours (right) at 80% *Cax*.

for the nominal case without tip clearance are presented first, in which some unsteady flow characteristics associated with three-dimensional vibration will be identified.

1. Nominal Case (Zero Tip Clearance)

The amplitudes and phase angles of the first harmonic pressure, presented in Figs. 7 and 8, are for the nominal case at an interblade phase angle of −60 deg. This particular interblade phase angle is chosen because it was identified to be the least stable interblade phase angle. The effects of the interblade phase angle on the blade stability will be discussed in the section on aerodynamic damping (Fig. 13).

Figure 7a shows the amplitude of the first harmonic pressure on the suction surface. Along the blade span, the amplitude of the first harmonic pressure consistently increases away from the hub except for the area toward the leading edge. However, the increase in the amplitude of the first harmonic pressure is not proportional to the increase in the local vibration amplitude along the span. In fact, the amplitude of the first harmonic pressure at 95% span is only about 2.5 times that at 10% span, whereas the local vibration amplitude at 95% span is 5 times that at 10% span. This nonproportional unsteady response to the local vibration amplitude at different blade spans certainly indicates that the unsteady flow response is of a strong three-dimensional nature. Because the baseline mean flow is largely of two-dimensional behavior, the three-dimensional unsteady flow effects are purely induced by the blade bending motion. On the pressure surface, displayed in Fig. 7b, a consistent increase in the amplitude along the span height is noticed for a range from 55%C to the trailing edge. Toward the leading edge, the change of the first harmonic pressure amplitude is not in a clear trend along the span on both surfaces. This behavior may be associated with a high sensitivity to the local incidence.

In Fig. 8a, the phase angle distributions of the first harmonic pressure along the chord are plotted at six span sections on the suction surface. Apart from the 95% span section, the phase angle shows consistent shift along the chord from 10–80% span. The phase angle becomes more diverse near the trailing edge, particularly at 10 and 95% span, which may suggest some 3-D endwall effects. Also, the influence of the imperfection of endwall sealing should be recognized. The phase angles on the pressure surface (Fig. 8b) are, on the whole, insensitive to the local span height.

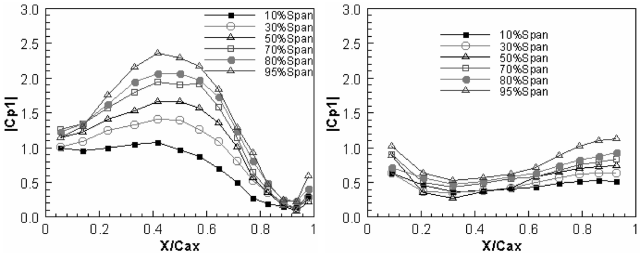

a) Suction surface **b) Pressure surface**

Fig. 7 First harmonic pressure amplitude (nominal case, IBPA = −60 deg).

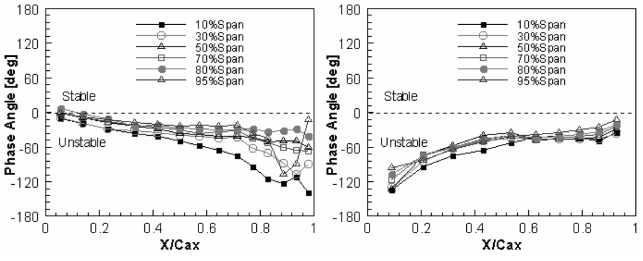

a) Suction surface **b) Pressure surface**

Fig. 8 First harmonic pressure phase angle (nominal case, IBPA = −60 deg).

2. Tip-Clearance Effects

Three tip-clearance settings of 1.25, 2.5, and 5%C have been investigated. In each case under investigation, the change in tip gap was applied to all blades in the cascade and not just the central oscillating blade. With the pressure tappings located close to the tip at a section of 95% span, the tip-clearance effects on the unsteady response can be readily identified locally in the tip region.

Figure 9 shows the amplitude of the first harmonic pressure at 95% span for an interblade phase angle of −60 deg, and Fig. 10 shows the corresponding phase angle. Differences in the amplitude of the first harmonic pressure are evident at 95% span on both the suction and pressure surfaces for the different tip configurations. When compared to the zero tip-clearance case, a frontal region of decreased unsteady pressure amplitude (up to 45%C) is observed for three tip-clearance settings, followed by a region of largely increased unsteady pressure amplitude (45–98%C), although slightly decreased pressure amplitude appears around 75%C for the tip-clearance setting of 1.25%C. The decrease of unsteady pressure amplitude in the frontal region is believed to be associated with the steady unloading on the suction surface, whereas the activity after the 45%C can be attributed to the steady reloading induced by the tip-clearance vortex. The rather erratic changes in amplitude of the tip clearance of 5%C are most likely associated with the largest steady reloading induced by the tip-clearance vortex, of which further observation from the phase angle will be made (Fig. 10a). On the pressure surface, shown in Fig. 9b, the amplitude of the first harmonic pressure decreases as the tip clearance increases for the region from 65%C to the trailing edge. This region corresponds to the steady reloading toward the trailing edge on the pressure surface. On the frontal chord (15–65%C), where a steady unloading appears, an increased amplitude is observed for the tip-clearance settings of 2.5 and 5%C, whereas the amplitude of the tip clearance of 1.25%C hardly differs from that of the zero tip clearance.

The phase angle distributions of the first harmonic pressure at 95% span on the suction surface for four tip-clearance settings is provided in Fig. 10a. The phase angles are almost identical for all four tip-clearance settings upstream of 40%C. Around midchord, the phase angle shifts toward 0 deg for three nonzero tip-clearance settings compared to the nominal setting, although this shift is not proportional to the size of the tip clearance. Indeed, the tip-clearance setting of 1.25%C has the biggest phase angle shift in this region. For

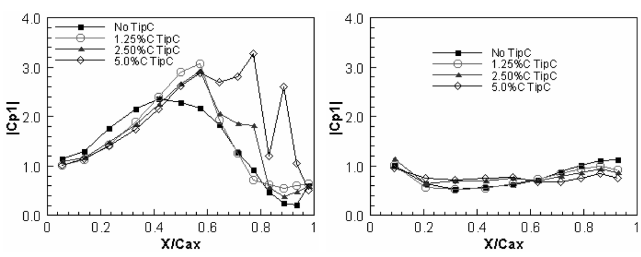

a) Suction surface **b) Pressure surface**

Fig. 9 First harmonic pressure amplitude at 95% span (IBPA = −60 deg).

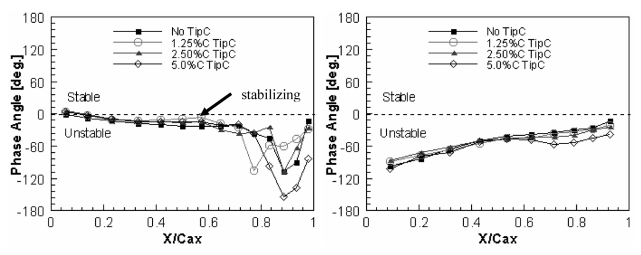

a) Suction surface **b) Pressure surface**

Fig. 10 First harmonic pressure phase angle at 95% span (IBPA = −60 deg).

the region toward the trailing edge, the biggest change in phase angle occurs for the tip-clearance setting of 5%C, which indicates a significant event related to the biggest steady reloading measured in this case. On the pressure surface (Fig. 10b), the unsteady response shows increased phase lag when the tip clearance increases for the rear half chord. On the frontal half chord, decreased phase lag is seen for tip clearances of 1.25 and 2.5%C, whereas not much difference can be observed for the tip clearance of 5%C.

Overall, the unsteady pressure response induced by the tip-clearance flow is concentrated on the suction surface.

3. *Aerodynamic Damping*

The "energy method" is the most commonly used technique to evaluate the aeroelastic stability of a blade. Simply speaking, the blade is unstable if the energy input from the surrounding flow is positive during a specific cycle of vibration. To use this method, the aerodynamic damping, which is a nondimensional parameter that directly indicates the energy exchange between the oscillating blade and its surrounding flow, is evaluated. The local aerodynamic damping is expressed in Eq. (2). The global aerodynamic damping is then obtained through integrating the local aerodynamic damping over the blade surface [Eq. (3)]

$$\xi_l = \frac{-\pi \cdot Ax_l |Cp_1| \sin(\phi_1)}{Ax_{\text{tip}}} \tag{2}$$

$$\xi = \frac{1}{h}\int_0^h \left(\frac{1}{C}\int_0^C \xi_l \mathrm{d}s\right)\mathrm{d}z \tag{3}$$

Figure 11 presents the local aerodynamic damping distribution at the interblade phase angle of −60 deg for four tip-clearance settings. The main regions of activity associated with the tip clearance are located above 50% span, most especially in the outer 20% span.

On the suction surface, two distinctive events are apparent. First, a negative damping alleviation is observed around midchord, toward the blade tip, for a small tip clearance of 1.25%C (event "A" as indicated in Fig. 11b). Second, an event developing in the region of flow diffusion is noticed. For a small tip clearance of 1.25%C (Fig. 11b), this event can be noticed at 80%C toward the blade tip, though still in its inception. As the tip clearance is increased, this event develops. For the tip-clearance setting of 5%C, it represents the dominant influence of the tip clearance (event "B" as indicated in Fig. 11d). The integrated aerodynamic damping at 95% span on the suction surface is displayed in Fig. 12, which gives an indication of the overall influence of these two events.

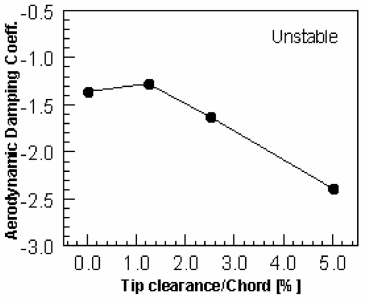

Fig. 12 Aerodynamic damping at 95% span (IBPA = −60 deg).

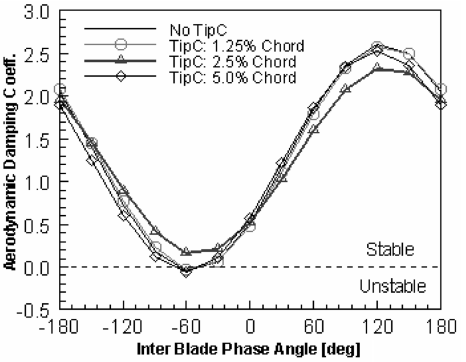

Fig. 13 Global aerodynamic damping.

Figure 13 shows the global aerodynamic damping for four different tip-clearance configurations. The least stable interblade phase angle, which has the smallest aerodynamic damping, is around −60 deg for this turbine cascade, although a slight difference manifests among different tip-clearance settings. This particular value interblade phase angle (−60 deg) was therefore chosen for the inspection of all unsteady pressure responses (previously presented).

For the small tip clearance (1.25%C), an overall stabilizing effect is found, though it is small. This stabilizing effect is mainly due to the alleviation on the negative damping around midchord toward the tip on the suction surface (Fig. 11b). For the medium tip clearance (2.5%C), considerable positive damping is induced on the pressure surface tip region, which makes the global damping of this setting stand out from the others. For the large tip clearance (5%C), a significant amount of negative damping (Fig. 11d) is generated in the flow diffusion region toward the trailing edge on the suction surface.

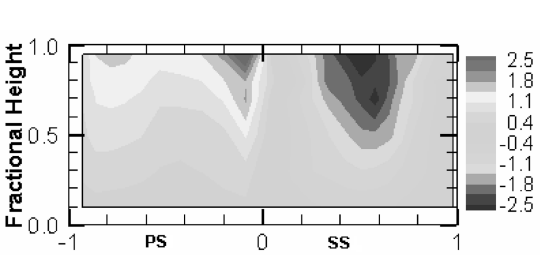

a) No tip clearance

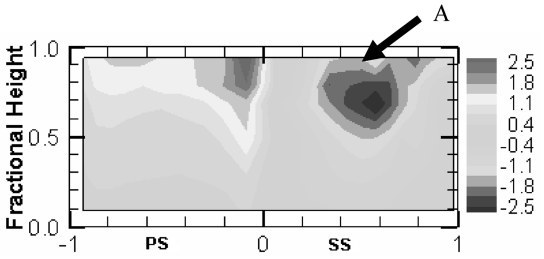

b) 1.25%C tip clearance

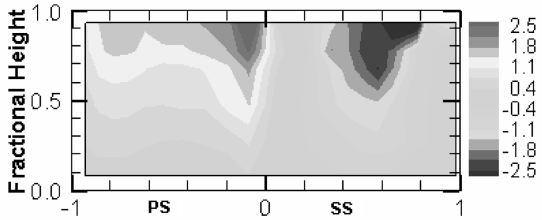

c) 2.5%C tip clearance

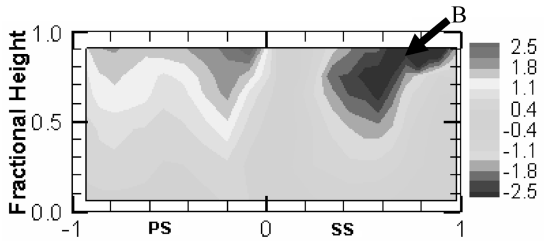

d) 5%C tip clearance

Fig. 11 Local aerodynamic damping (IBPA = −60 deg).

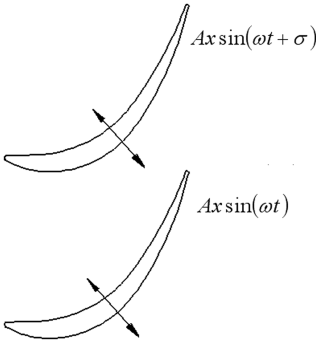

Fig. 14 Oscillating turbine passage.

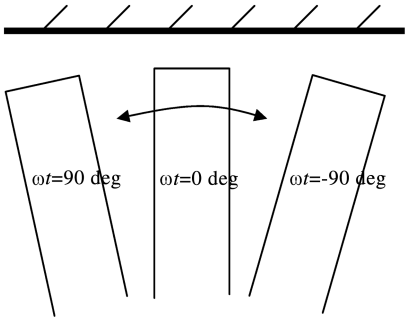

Fig. 15 Blade tip at the minimum, mean, and maximum displacements (axial view).

However, this effect is offset by the increased positive damping on the pressure surface, and only a minor change in global aerodynamic damping can be observed when compared to the zero tip-clearance case.

4. Further Discussion (Quasi-Steady Analysis)

A simple analysis is presented here to help understand the apparent stabilizing behavior on the suction surface at a small tip clearance (event A as indicated in Fig. 11b). Consider a turbine blade passage oscillating in a flapping mode (positive downward) with an interblade phase angle σ, as shown in Fig. 14. The lower blade is the reference blade on which the aerodynamic work done by the fluid to the blade in one vibration period is given by

$$W = \pi A_f \cdot A_x \sin(\phi_{fx}) \tag{4}$$

where A_f is the amplitude of the unsteady force F on the reference blade in the vibration direction, and ϕ_{fx} is the phase lead of the force to the vibration motion, that is to say,

$$F = A_f \sin(\omega t + \phi_{fx}) \tag{5}$$

If varying quasi steadily, the blade loading F is inversely proportional to blade solidity. Hence, F is expected to be proportional to the blade-to-blade spacing:

$$F \propto [A_x \sin(\omega t) - A_x \sin(\omega t + \sigma)] \tag{6}$$

At the zero frequency limit, we have

$$F \propto -A_x \sin(\sigma) \tag{7}$$

This shows that quasi-steady unsteady loading induced by the flapping vibratory motion should be in phase with the interblade phase angle σ, but with a negative sign. Consequently, we have the maximum work done to blade (i.e., maximum magnitude of negative damping) when the interblade phase angle is -90 deg. Note that for a turbine this corresponds to a backward traveling wave. The same argument applies to a compressor, for which the most unstable mode corresponds to a forward traveling wave at 90 deg IBPA.

This quasi-steady argument on a 2-D blade-to-blade section can now be used as a basis to explain the stabilizing behavior of a small tip clearance (Fig. 11b). A sketch of a tip gap (viewed from the axial direction) is given in Fig. 15 for the three positions during a vibration period.

The 2-D quasi-steady analysis presented earlier leads to the observation that for the most unstable IBPA (-90 deg), the maximum unsteady blade force would occur at the mean position ($\omega t = 0$ deg). However, this phasing for the maximum blade force would be affected by the tip clearance. The steady results (Fig. 5) clearly show that the suction loading near the tip varies directly with the clearance gap. It follows that, during one vibration cycle, the maximum loading should occur at the phase angle with a maximum tip gap. Clearly, we can see from Fig. 15 that the mean displacement position $\omega t = 0$ deg corresponds to the minimum tip gap. Hence, the maximum loading due to the tip clearance is not in phase with that due to the blade-to-blade vibratory displacement at the most unstable IBPA. This phase offset should explain why it is possible to have a stabilizing effect with a tip clearance. The reason for the most pronounced effect at a small tip clearance may simply be because the relative tip gap variation during one vibration cycle is proportionally larger when the mean tip clearance is small.

At a large tip clearance, the tip vortex is already well developed (highly concentrated), as indicated in Fig. 6c. Now an increase in the blade-to-blade spacing would no longer lead to any further strengthening of the tip vortex (the local flow turning and its associated low pressure). Hence, the maximum local low pressure peak at 80%C on the suction surface happens at $\omega t = 0$ deg, leading to a local destabilizing region (event B as indicated in Fig. 11d).

IV. Conclusions

An experimental investigation into the influence of the tip-clearance flow on the aerodynamic damping characteristics in a turbine cascade has been conducted. Extensive steady and unsteady measurements of blade surface pressure were presented and discussed for a tip-clearance range from 0–5%C. The steady pressure data compared well with CFD simulations obtained using a simple tip-clearance model. The test data demonstrates a strong three-dimensional behavior of the unsteady flow induced by the blade vibration. The radial redistribution of unsteady response is evident.

Regarding the influence of tip clearance, both experimental and CFD results for steady flow indicate a significant role played by the tip leakage vortex. For small tip clearances (1.25 and 2.5%C), the tip gap variation during blade oscillation provides a stabilizing contribution around the midchord on the suction surface near the tip. However, for a large tip clearance (5%C), this stabilizing contribution is largely offset by a destabilizing contribution measured around 80%C, which is associated with a well developed tip-clearance vortex.

Acknowledgments

This work has been supported in part by ALSTOM Power Ltd, which is gratefully acknowledged. The authors would also like to thank Peter Walker for many useful technical discussions. This paper was presented at ASME Turbo Expo, 8–12 May 2006, Barcelona, Spain, Paper GT2006-90541.

References

[1] Bell, D. L., and He, L., "Three-Dimensional Unsteady Flow for an Oscillating Turbine Blade and the Influence of Tip Leakage," *Journal of Turbomachinery*, Vol. 122, No. 1, 2000, pp. 93–101. doi:10.1115/1.555432

[2] Norryd, M., and Bölcs, A., "Experimental Investigation of Unsteady Pressure Behaviors in a Linear Turbine Cascade," *The 8th International Symposium on Unsteady Aerodynamics and Aeroelasticity of Turbomachines*, Kluwer, Dordrecht, The Netherlands, Sept. 1997.

[3] Sanders, A. J., Hassan, K. K., and Rade, D. C., "Experimental and Numerical Study of Stall Flutter in a Transonic Low-Aspect Ratio Fan Blisk," *Journal of Turbomachinery*, Vol. 126, No. 1, 2004, pp. 166–174.

doi:10.1115/1.1645532
[4] Hanamura, Y., Tanaka, H., and Yamaguchi, Y., "A Simplified Method to Measure Unsteady Forces Acting on the Vibrating Blades in a Cascade," *Bulletin of the JSME*, Vol. 23, No. 180, 1980, pp. 880–887.
[5] Crawley, E. F., "Aeroelastic Formulations for Turbomachines and Propellers," *Proceedings of the Third International Symposium on Unsteady Aerodynamics of Turbomachines and Propellers*, Cambridge Univ. Press, Cambridge, England, U.K., 1984, pp. 13–28.
[6] Fransson, T. H., "Analysis of Experimental Time-Dependent Blade Surface Pressure from an Oscillating Turbine Cascade with the Influence Coefficient Technique," ASME Paper 90-GT-225, 1990.
[7] Buffum, D. H., and Fleeter, S., "Effect of Wind Tunnel Acoustic Modes on Linear Oscillating Cascade Aerodynamics," *Journal of Turbomachinery*, Vol. 116, No. 3, 1994, pp. 513–524.
[8] Körbächer, H., and Bölcs, A., "Steady-State and Time-Dependent Experimental Results of a NASA-3506 Cascade in an Annular Channel," ASME Paper 96-GT-334, 1996.
[9] He, L., "Unsteady Flow in Oscillating Turbine Cascades: Part 1—Linear Cascade Experiment," *Journal of Turbomachinery*, Vol. 120, No. 2, 1998, pp. 262–268.
[10] Nowinski, M., and Panovsky, J., "Flutter Mechanisms in Low Pressure Turbine Blades," *Journal of Engineering for Gas Turbines and Power*, Vol. 122, No. 1, 2000, pp. 82–88.
doi:10.1115/1.483179
[11] Yang, H., and He, L., "Experimental Study on Linear Compressor Cascade with Three-Dimensional Blade Oscillation," *Journal of Propulsion and Power*, Vol. 20, No. 1, 2004, pp. 180–188.
[12] Vogt, D. M., "Experimental Investigation of Three-Dimensional Mechanisms in Low-Pressure Turbine Flutter," Ph.D. Thesis, Royal Institute of Technology, Sweden, 2005.
[13] Irwin, H. P. A. H., Cooper, K. R., and Girard, R., "Correction of Distortion Effects Caused by Tubing Systems in Measurements of Fluctuation Pressures," *Journal of Industrial Aerodynamics*, Vol. 5, 1979, pp. 93–107.
doi:10.1016/0167-6105(79)90026-6
[14] Sims-Williams, D. R., "Self-Excited Aerodynamic Unsteadiness Associated with Passenger Cars," Ph.D. Thesis, School of Engineering, Univ. of Durham, Durham, U.K., 2001.
[15] He, L., "Three-Dimensional Unsteady Navier–Stokes Analysis of Stator-Rotor Interactions in Axial-Flow Turbines," *Proceedings of the Institution of Mechanical Engineers, Part A: Journal of Power and Energy*, Vol. 214, No. 1, 2000, pp. 13–22.
doi:10.1243/0957650001537813
[16] Dawes, W. N., "A Numerical Analysis of the Three-Dimensional Viscous Flow in a Transonic Compressor Rotor and Comparison with Experiment," *Journal of Turbomachinery*, Vol. 109, No. 1, 1987, pp. 83–90.
[17] Storer, J. A., and Cumpsty, N. A., "Tip Leakage Flow in Axial Compressors," *Journal of Turbomachinery*, Vol. 113, No. 2, 1991, pp. 252–259.
[18] Van Zante, D. E., Strazisar, A. J., Wood, J. R., Hathaway, M. D., and Okiishi, T. H., "Recommendations for Achieving Accurate Numerical Simulation of Tip Clearance Flows in Transonic Compressor Rotors," *Journal of Turbomachinery*, Vol. 122, No. 4, 2000, pp. 733–742.
doi:10.1115/1.1314609
[19] Walker, M., Gregory-Smith, D., and He, L., "A Study of Large Tip Clearance in A Row of Low Speed Compressor Blades," *6th European Conference on Turbomachinery, Fluid Dynamics and Thermodynamics*, March 2005.

C. Tan
Associate Editor